Proceedings of the 4th International Conference on Functional Materials and Civil Engineering
DOI: 10.54254/2755-2721/2026.38955

Influence of Relative Thickness on the Aerodynamic Performance of NACA 24-Series Airfoils at Low Reynolds Numbers

Dongxian Yang

Department of Vehicle Engineering, Jiamusi University, Jiamusi, China
Y3350345771@outlook.com

Abstract. This paper compares saved steady two-dimensional SST k–ω calculations for NACA 2412, NACA 2415, and NACA 2418 at a nominal Reynolds number of 2.09×10^6 and nominal angles of attack from 0° to 16°. The profiles share 2% camber at 40% chord and have thickness ratios of 12%, 15%, and 18%. Final-iteration lift, drag, pitching moment, and lift-to-drag ratio are traced to the case/data files and coefficient histories. In this dataset, minimum drag increases with thickness, while NACA 2412 has the highest lift-to-drag ratio and NACA 2418 the lowest drag at the largest nominal incidence. The saved meshes contain only 38–41 airfoil-wall faces. Residual and force histories do not demonstrate strict iterative convergence, and the horizontal symmetry boundaries constrain the inclined inflow. These limitations may affect both the coefficient magnitudes and the profile ranking. The results therefore describe the archived numerical response; grid and boundary sensitivity studies, improved convergence, and traceable experimental comparisons are required before quantitative design conclusions can be drawn.

Keywords: NACA 24-series airfoil, relative thickness, aerodynamic performance, k–ω SST turbulence model, low Reynolds number

1. Introduction

Airfoil geometry determines how pressure forces and viscous forces develop on a lifting surface. That relationship matters for aircraft wings, wind-turbine blades, and marine control surfaces because it affects both efficiency and the usable operating range [1]. Relative thickness is especially important: it supplies structural volume, changes the surface curvature, and consequently modifies the pressure field that produces lift and drag [2]. The NACA four-digit family remains useful for controlled comparisons because its geometry is simple to generate and its aerodynamic behavior is documented in the NACA data literature [3].

A change in thickness affects more than the maximum distance between the upper and lower surfaces. It alters the leading-edge radius, the rate at which the flow accelerates over the nose, and the pressure recovery toward the trailing edge. A thicker section also has more wetted area and provides greater internal depth for spars, skins, or other structural components. These effects pull the design in different directions. Structural depth may be useful, while the associated pressure and

© 2026 The Authors. This is an open access article distributed under the terms of the Creative Commons Attribution License 4.0 (https://creativecommons.org/licenses/by/4.0/).

DOI: 10.54254/2755-2721/2026.38955

viscous changes can reduce aerodynamic efficiency. The balance becomes especially important when viscous forces form a noticeable part of the total drag [1, 2].

The four digits of a NACA designation encode the basic section geometry. The first digit gives maximum camber in percent of chord, the second identifies the camber location in tenths of chord, and the final two digits give thickness in percent of chord [2]. For the 24-series, the camber remains 2% at 40% chord. Replacing 2412 with 2415 and then 2418 therefore changes the thickness while holding the camber distribution fixed, which makes the family suitable for isolating thickness effects.

Keeping the camber line unchanged gives the comparison a clear physical basis. If camber, camber position, and thickness were varied together, a change in lift could not be attributed to one geometric parameter with confidence. The NACA 2412, 2415, and 2418 profiles avoid that ambiguity because the change is confined to the thickness distribution. The arrangement does not represent every choice made during practical wing design, but it provides a controlled way to identify how thickness modifies the response of an otherwise related group of sections [4, 5].

Previous work provides several useful reference points for this comparison. The Abbott and von Doenhoff compilation remains a standard source of airfoil data [2]. Gao et al. reported incidence-dependent changes in lift-to-drag ratio for NACA 4412, 4415, and 4418 [4]. Keskin et al. investigated the effect of thickness on flow over cambered airfoils [5]. Ma et al. focused on low-Reynolds-number behavior, including the sensitivity of thin profiles to laminar separation bubbles [6]. Other studies have applied data-driven models to airfoil analysis [7].

Results reported in the literature are not always directly comparable. Reynolds number, surface condition, transition treatment, turbulence closure, computational-domain size, and angle-of-attack spacing can all influence the reported coefficients. One paper may emphasize maximum lift, while another focuses on drag or separation behavior. The present work therefore uses earlier studies to establish physical expectations rather than combining their numerical values as though they came from one experiment. A common solver setup facilitates comparison [4-7], but shared numerical settings do not demonstrate that either the absolute coefficients or their relative ordering are accurate.

The analysis connects the force coefficients with the surface quantities that produce them. Lift and drag describe the overall aerodynamic response, but they do not show where the loading changes along the chord. Pressure coefficient and skin-friction coefficient provide that local information. Pitching moment adds a measure of how the pressure distribution influences longitudinal balance. Reading these quantities together helps distinguish a genuine thickness effect from a change that appears in only one integrated coefficient.

The present comparison addresses a narrower gap. The three 24-series sections are evaluated with the same computational setup, approximately the same Reynolds number, and the same nominal incidence range. This makes it possible to examine lift, drag, efficiency, and pitching moment together instead of treating each quantity in isolation. The sources have distinct roles: NACA Technical Report 824 provides experimental aerodynamic data [3], while the University of Illinois Urbana-Champaign (UIUC) Airfoil Coordinates Database provides geometry reference coordinates [8].

The study compares saved calculations for NACA 2412, NACA 2415, and NACA 2418 at nominal $Re = 2.09 \times 10^6$ over 0°–16°. The analysis covers force coefficients, lift-to-drag ratio, surface pressure and skin friction, and pitching moment. NACA TR-824 supplies experimental context [3], while UIUC supplies geometry reference coordinates [8]. The comparisons are interpreted subject to the documented mesh, outer-boundary, and iterative-convergence limitations.

DOI: 10.54254/2755-2721/2026.38955

2. Research methodology

2.1. Geometric model

The section geometry is generated from the NACA four-digit construction: a camber line is combined with a thickness distribution measured normal to that line [1]. For the 24-series, the camber line consists of two quadratic branches. For $0 \le x/c \le p$, $z_c/c = (m/p^2)(2p(x/c) - (x/c)^2)$; for $p \le x/c \le 1$, $z_c/c = (m/(1-p)^2)((1-2p) + 2p(x/c) - (x/c)^2)$. Here m is maximum camber as a fraction of chord and p is its chordwise location; the present models use $m = 0.02$ and $p = 0.40$.

The standard four-digit thickness polynomial is $y_t/c = (t/0.20)(0.2969\sqrt{(x/c)} - 0.1260(x/c) - 0.3516(x/c)^2 + 0.2843(x/c)^3 - 0.1015(x/c)^4)$. With $\theta = \arctan(dz_c/dx)$, the surface coordinates are $x_u = x - y_t \sin\theta$, $z_u = z_c + y_t \cos\theta$, $x_l = x + y_t \sin\theta$, and $z_l = z_c - y_t \cos\theta$ [2]. With t = 0.12, 0.15, and 0.18, the resulting sections are NACA 2412, NACA 2415, and NACA 2418. The nominal chord is 1.0 m; geometric sampling and the final surface-mesh resolution are distinct. Table 1 lists the resulting geometric parameters.

Coordinates are normalized by the nominal chord before meshing. The geometry definition in Table 1 specifies the intended camber and thickness ratios; the final case files determine the discretization actually used by the solver. Those files contain 38, 39, and 41 wall faces for NACA 2412, 2415, and 2418, respectively. A dense coordinate list used to construct a curve does not guarantee a comparably fine computational surface mesh.

The geometry in Table 1 shows the controlled nature of the comparison. Maximum camber remains 2% of chord and its location remains 40% of chord, whereas relative thickness increases in equal three-percentage-point steps. The sequence from NACA 2412 to NACA 2418 therefore changes both the nose radius and the thickness of the rear part of the profile without moving the camber peak. This distinction is useful when the pressure and drag trends are discussed later [2].

Table 1. Geometric parameters of the NACA 24-series airfoils investigated in the present study

Airfoil	Maximum camber (%c)	Camber position (%c)	Relative thickness (%c)
NACA 2412	2	40	12
NACA 2415	2	40	15
NACA 2418	2	40	18

2.2. Mesh generation

The quadrilateral-dominant meshes contain 51,181, 51,126, and 51,232 cells for NACA 2412, 2415, and 2418, respectively. Each profile uses the same mesh at its five nominal incidences. The corresponding airfoil-wall face counts are 38, 39, and 41, with edge lengths of 13.51–107.06 mm, 17.06–107.92 mm, and 13.22–108.98 mm. Thus the saved surface meshes do not realize a 5 mm spacing. Outer-boundary edges are approximately 0.1 m. The domain extends from x = −10 m to 15 m and from y = −10 m to 10 m, with a nominal 1 m chord.

The domain provides a nominal 10-chord upstream extent and 14-chord downstream extent. However, distance from the airfoil alone does not establish boundary independence. For nonzero incidence, the inlet includes a vertical velocity component while the horizontal upper and lower boundaries impose zero normal velocity. These constraints cannot preserve a uniform inclined far

DOI: 10.54254/2755-2721/2026.38955

field. The domain dimensions are common to the cases, but their influence on the forces and profile ordering has not been quantified.

Wall-normal inflation layers are present. Geometric checks at several NACA 2412 wall locations give a first-layer height near 5.0×10^{-5} m, with local thin-layer growth near 1.15 and a nonuniform transition to the outer mesh. The saved mesh does not establish a uniform 15-layer stack with growth 1.2. Figure 1 shows the NACA 2418 mesh. For its highest nominal incidence, the wall-length-weighted y^+ is 1.863 and the maximum is 3.594; Figure 2 illustrates the wall distribution.

The reported y^+ values characterize wall-normal resolution for the SST calculation [9]. In a two-dimensional model of unit depth, wall-length weighting is equivalent to area weighting. The mean y^+ of about 1.86 for NACA 2418 at the highest nominal incidence does not establish adequate chordwise resolution. Surface discretization and the transition from thin wall layers to the outer mesh remain separate concerns.

A formal grid-refinement study is not available for this dataset. With only 38–41 airfoil-wall faces, the pressure and shear distributions require additional spatial-resolution checks. Using broadly similar grids for the three profiles does not guarantee cancellation of discretization errors. The coefficient magnitudes and thickness ranking are consequently treated as provisional until surface, wake, and wall-layer refinement have been assessed.

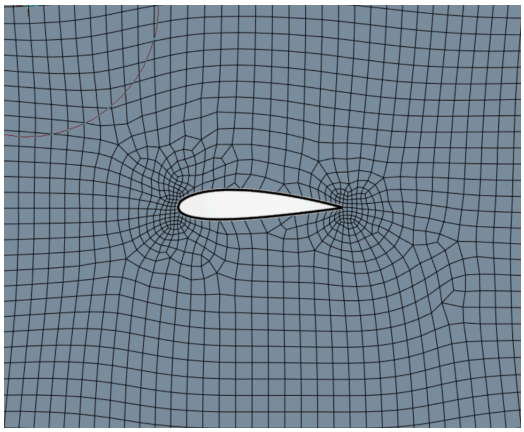


Figure 1. Computational grid around the NACA 2418 airfoil

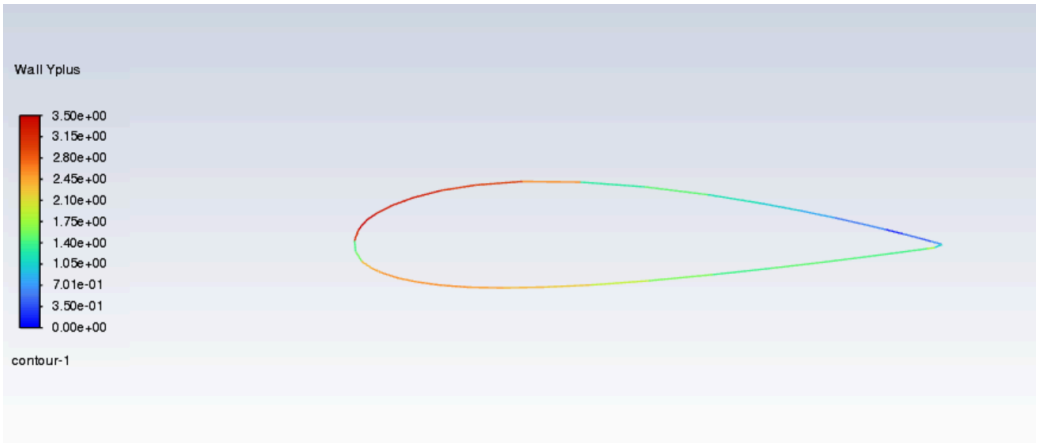


Figure 2. Wall y^+ on NACA 2418 at nominal $\alpha = 16°$ and $Re \approx 2.09 \times 10^6$; the saved inlet angle is 15.857° and the wall-length-weighted mean y^+ is 1.863

DOI: 10.54254/2755-2721/2026.38955

2.3. Boundary conditions

The simulations use ANSYS Fluent; Ives et al. provide a prior NACA 2412 application [10]. A steady two-dimensional Reynolds-averaged Navier–Stokes formulation is closed with the shear-stress-transport (SST) k–ω model [9]. The model blends the near-wall behavior of the k–ω formulation with the outer-flow behavior of the k–ε formulation, which is useful for separated flows and adverse pressure gradients [9].

The SST formulation is selected because the present flow contains both a wall-bounded boundary layer and an adverse pressure gradient over the upper surface. Its k–ω behavior near the wall avoids dependence on a wall function at the reported y^+ level, while the outer-flow blending limits the sensitivity of the freestream solution [9]. This choice is suitable for comparing attached and moderately separated conditions. It does not remove the limitations of a steady Reynolds-averaged approach: transient separation, vortex shedding, and cycle-to-cycle changes near stall are not resolved by the steady solution.

The reference speed is 30.544 m/s, with a nominal Mach number of about 0.09. Air density is 1.225 kg/m^3 and dynamic viscosity is 1.7894×10^{-5} Pa·s. The 1 m reference chord gives Re ≈ 2.09×10^6. Operating pressure is 101325 Pa; outlet gauge pressure is zero. The reference temperature is 288.16 K, and the air model uses constant density and viscosity. The inlet turbulence intensity is 1% and the turbulent-viscosity ratio is 10. Nominal incidence is varied through the inlet velocity components at 0°, 4°, 8°, 12°, and 16°.

The saved inlet components correspond closely to the nominal incidences, except that the NACA 2418 case labelled 16° uses u = 29.3689 m/s and v = 8.34191 m/s, giving 15.857°; the other two 16° cases are near 15.996°. Figures and tables retain the nominal labels. Horizontal symmetry boundaries constrain the vertical flow, so the inlet angle should not be assumed to remain uniform throughout the domain. The coarse incidence spacing, grid resolution, and incomplete convergence prevent a reliable stall-angle determination.

The airfoil wall is stationary and no-slip. The steady pressure-based solver uses Coupled pressure–velocity coupling, second-order pressure interpolation, second-order upwind discretization for momentum, k, and ω, and least-squares cell-based gradients. C_l and C_d are evaluated normal and parallel to the inlet direction; C_m is taken about (x/c, y/c) = (0.25, 0) with a positive z axis. The reference area and depth are 1 m^2 and 1 m. Table 2 summarizes the saved settings.

The data are final-iteration values: the saved iteration is 4000 for 14 cases and 4239 for NACA 2415 at 8°. The residual settings specify an absolute criterion of 10^{-3}, but the final continuity and ω residuals exceed this value in every case. Although the velocity residuals are below 10^{-6}, strict convergence of all equations is not demonstrated. For NACA 2412 at 16°, the last-500-iteration ranges of C_l and C_d are 9.63% and 10.40% of their means. These fluctuations are iterative uncertainty; an average over steady iterations would not be a physical time average.

Table 2. Summary of boundary conditions and numerical settings employed in the present simulations

Parameter	Value / Setting
Turbulence model	SST k–ω
Reynolds number	Approximately 2.09×10^6
Nominal Mach number	0.09
Nominal angle of attack	0°, 4°, 8°, 12°, 16°; see inlet-angle qualification

DOI: 10.54254/2755-2721/2026.38955

Table 2. (continued)

Inlet condition	Velocity components; reference speed 30.544 m/s
Outlet condition	Pressure outlet, zero gauge pressure
Top/bottom boundaries	Horizontal symmetry; boundary sensitivity unresolved
Wall condition	Stationary, no-slip
Pressure–velocity coupling	Pressure-based Coupled
Spatial discretization	Second-order upwind (momentum, k, ω)
Pressure interpolation	Second-order
Gradient method	Least squares cell based
Iteration and convergence status	Final iteration 4000 or 4239; strict convergence not demonstrated
First layer height (NACA 2412 check)	Approximately 5.0×10^{-5} m at sampled locations
Inflation geometry (NACA 2412 check)	Local growth near 1.15; layer count varies

2.4. Aerodynamic parameter formulas

The following dimensionless quantities are used to report the aerodynamic response. Lift is normalized by freestream dynamic pressure and the reference area, taken here as chord times unit span:

$$C_l = \frac{L}{½\rho V_\infty^2 c} \tag{1}$$

In Equation (1), C_l is the dimensionless lift coefficient, L is lift force per unit span (N/m), ρ is air density (kg/m^3), V_∞ is freestream velocity (m/s), and c is chord length (m).

Drag coefficient is defined with the drag force in place of lift:

$$C_d = \frac{D}{½\rho V_\infty^2 c} \tag{2}$$

In Equation (2), C_d is the dimensionless drag coefficient and D is drag force per unit span (N/m). The symbols ρ, V_∞, and c retain the definitions and units given for Equation (1).

Aerodynamic efficiency is represented by the ratio of lift coefficient to drag coefficient:

$$K = \frac{C_l}{C_d} \tag{3}$$

In Equation (3), K is the dimensionless lift-to-drag ratio calculated from C_l and C_d as defined in Equations (1) and (2).

The Reynolds number used to characterize the flow is calculated from density, velocity, chord, and dynamic viscosity:

$$Re = \frac{\rho V_\infty c}{\mu} \tag{4}$$

DOI: 10.54254/2755-2721/2026.38955

In Equation (4), Re is the dimensionless Reynolds number and μ is dynamic viscosity (Pa·s). The quantities ρ (kg/m^3), V_∞ (m/s), and c (m) follow Equation (1).

Surface pressure is expressed in nondimensional form through the pressure coefficient:

$$C_p = \frac{(p-p_\infty)}{½\rho V_\infty{}^2} \tag{5}$$

In Equation (5), C_p is the dimensionless pressure coefficient, p is local static pressure (Pa), p_∞ is freestream static pressure (Pa), V_∞ is freestream velocity (m/s), and ρ is air density (kg/m^3).

Wall shear is normalized by freestream dynamic pressure to obtain the skin-friction coefficient:

$$C_f = \frac{\tau_w}{½\rho V_\infty{}^2} \tag{6}$$

In Equation (6), C_f is the dimensionless skin-friction coefficient and τ_w *is the signed tangential wall shear stress acting on the airfoil (Pa), positive along the local surface tangent toward increasing x.* Air density and freestream velocity retain the units given for Equations (1) and (5).

The pitching moment about the quarter-chord is reported with the following coefficient:

$$C_m = \frac{M}{½\rho V_\infty{}^2 c^2} \tag{7}$$

In Equation (7), C_m is the dimensionless pitching-moment coefficient and M is pitching moment per unit span about the quarter-chord (N·m/m). The remaining quantities retain the definitions and units given for Equation (1).

These coefficients form the basis for the comparisons; the reported integrated values are taken at the final saved iteration.

The common normalization makes the results independent of the dimensional force scale used by the two-dimensional model. Because the reference area is chord times unit span, C_l and C_d can be compared directly among the three profiles. The ratio K is useful for judging efficiency, although it must be interpreted together with its separate lift and drag terms. C_p identifies the chordwise pressure loading, C_f indicates the local wall-shear contribution, and C_m shows how the distributed load acts about the quarter-chord reference. These local and integrated measures are therefore complementary rather than interchangeable.

3. Results and discussion

3.1. Lift coefficient analysis

Figure 3 shows that the first part of the lift curve is similar for all three profiles. From 0° to 8°, C_l increases steadily. NACA 2415 has the largest average slope in this interval, whereas NACA 2418 has the smallest. Camber keeps the zero-incidence lift positive: the calculated values are about 0.20, 0.13, and 0.14 for NACA 2412, 2415, and 2418, respectively.

The tabulated increments reveal that the thickness effect is not a simple constant offset. Between 0 degrees and 8 degrees, C_l rises by 0.124 for NACA 2412, by 0.161 for NACA 2415, and by only 0.063 for NACA 2418. Over the final interval from 12 degrees to 16 degrees, the increases are 0.138, 0.124, and 0.115, respectively. NACA 2415 therefore approaches the NACA 2412 lift level as incidence increases, whereas NACA 2418 remains clearly lower. This describes the saved dataset; the unresolved numerical sensitivities prevent attributing the full difference to thickness.

DOI: 10.54254/2755-2721/2026.38955

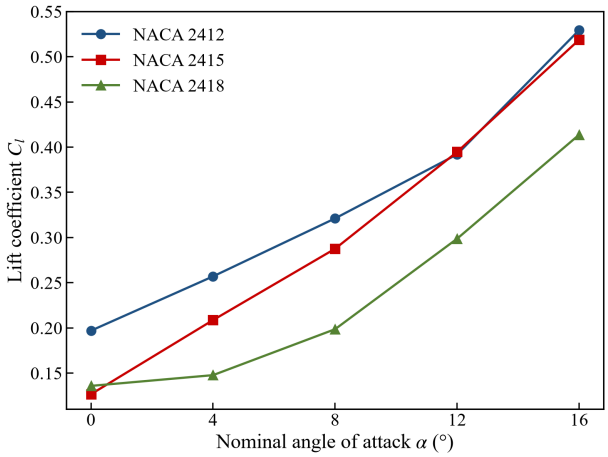


Figure 3. Variation of lift coefficient with nominal angle of attack for the NACA 2412, 2415, and 2418 airfoils at Re = 2.09×10^6

The curves separate more clearly above 10°. At 8°, C_l is 0.32 for NACA 2412, 0.29 for NACA 2415, and 0.20 for NACA 2418. At 16°, the corresponding values are approximately 0.53, 0.52, and 0.41. NACA 2412 and NACA 2415 remain close over most of the range, while NACA 2418 produces the lower lift coefficient. No downturn appears in the sampled lift values, but these calculations do not establish the stall angle. Selected final-iteration values are listed in Table 3.

Thickness changes the leading-edge curvature and the pressure distribution, but the resulting separation behavior depends on Reynolds number and incidence. Gao et al. studied NACA 44-series sections [4], whereas Keskin et al. examined NACA 24-series sections at lower Reynolds numbers than the present simulations [5]. These sources establish relevant mechanisms rather than directly validating the present coefficient values.

The pressure explanation also clarifies why a thicker profile does not automatically produce more lift. Added thickness changes the curvature that establishes the suction-side acceleration, but lift depends on the pressure difference integrated over the complete surface. The upper- and lower-surface pressure distributions must both be considered; a single suction peak does not determine total loading. Boundary-layer behavior modifies that loading further at higher incidence. Geometry, pressure recovery, and viscous response provide possible mechanisms [4, 5]; the present numerical limitations prevent a quantitative attribution of the observed trends.

Table 3. Final-iteration lift coefficients at nominal angles of attack

α (°)	C_l (NACA 2412)	C_l (NACA 2415)	C_l (NACA 2418)
0	0.197	0.127	0.136
4	0.257	0.209	0.148
8	0.321	0.288	0.199
12	0.392	0.395	0.299
16	0.530	0.519	0.414

DOI: 10.54254/2755-2721/2026.38955

3.2. Drag coefficient analysis

Figure 4 shows the lowest drag at 0° and increasing drag with incidence. The minimum C_d values are about 0.014, 0.016, and 0.021 for NACA 2412, 2415, and 2418. Geometry-dependent drag is also discussed in [2, 11]; the present results do not separate pressure drag from skin-friction drag.

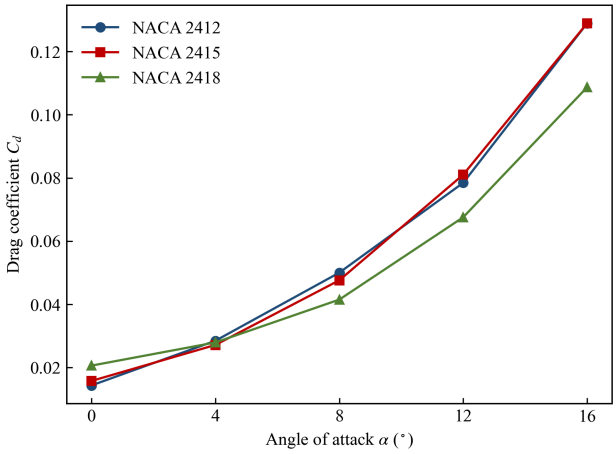


Figure 4. Variation of drag coefficient with nominal angle of attack for the NACA 2412, 2415, and 2418 airfoils at Re = 2.09×10^6

The saved drag values rise more rapidly after nominal 8°; the contribution of separation to this increase has not been isolated. NACA 2412 shows the sharpest increase near the upper end of the range. At 16°, C_d is approximately 0.129 for NACA 2412, 0.129 for NACA 2415, and 0.109 for NACA 2418. These statements apply only to the calculated 0°–16° interval.

The ordering of the profiles changes with incidence. At 0 degrees, NACA 2418 has a minimum drag coefficient of 0.0206, about 44% higher than the 0.0143 value for NACA 2412. At 16 degrees, the NACA 2418 value is 0.1087, roughly 16% below the NACA 2412 value of 0.1289. These are differences within the saved calculations. Their physical magnitude and ordering require verification because grid resolution, boundary constraints, and incomplete convergence can affect the apparent thickness trend.

Figure 5 is reconstructed from the saved wall-face pressures at nominal 8°, using the common reference dynamic pressure. NACA 2418 has the most negative sampled upper-surface C_p, approximately −0.787, compared with −0.726 for NACA 2415 and −0.660 for NACA 2412. Upper and lower surface values are plotted separately. These coarse samples do not determine the true suction-peak magnitude or location, and a single peak cannot determine the integrated lift.

The wall-face pressure values and signed wall-shear contributions provide a traceable connection between the local and integrated quantities. For NACA 2412 at 0° and 16°, independent integration reproduces the stored C_l, C_d, and C_m within numerical roundoff. This checks the reporting convention, not the physical accuracy of the solution. Ma et al. [6] studied separation bubbles at Re = 5×10^5; the present fully turbulent SST model does not resolve transition explicitly.

DOI: 10.54254/2755-2721/2026.38955

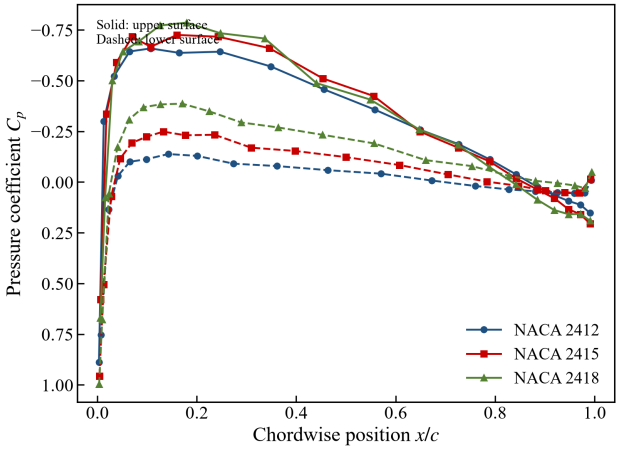


Figure 5. Saved wall-face C_p at nominal α = 8° and Re ≈ 2.09 × 10^6. Solid and dashed lines connect upper- and lower-surface samples, respectively

3.3. Lift-to-drag ratio analysis

Figure 6 compares *K* with incidence. For each profile, the ratio is highest at 0° and decreases as drag grows toward the upper end of the calculation. The three curves share this overall shape, but their peak levels differ with the saved lift and drag values; the numerical sensitivities have not been separated from the geometry effect.

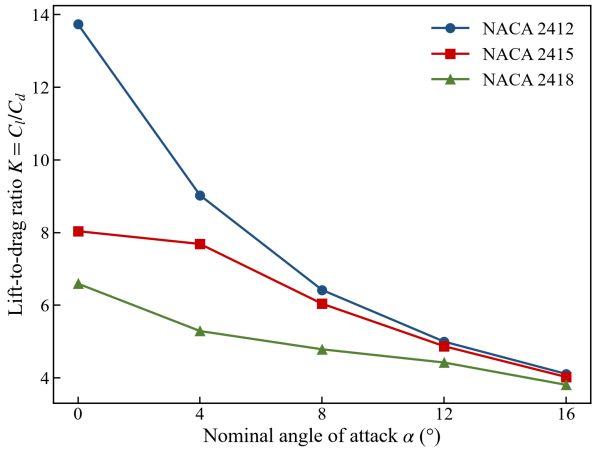


Figure 6. Variation of lift-to-drag ratio with nominal angle of attack for the NACA 2412, 2415, and 2418 airfoils at Re = 2.09 × 10^6

NACA 2412 gives the largest calculated K, about 13.7 at 0°. The peak values for NACA 2415 and NACA 2418 are about 8.0 and 6.6. Between 0° and 8°, the ratio falls from 13.7 to 6.4 for NACA 2412 and from 6.6 to 4.8 for NACA 2418. Thus the saved thicker-profile cases have lower K in this nominal low-incidence interval, subject to the numerical limitations.

At nominal 16°, K is 4.11, 4.02, and 3.81 for NACA 2412, 2415, and 2418. The separation between the curves is smaller than at 0°. This ranking is descriptive of the saved cases and should not yet be used to select an airfoil. Boundary and grid sensitivity, iterative fluctuations, and the

DOI: 10.54254/2755-2721/2026.38955

slightly different inlet angle for NACA 2418 need to be resolved before differences of this size can support a design decision.

Figure 7 presents the moment coefficient about the quarter-chord. The reported C_m values generally decrease with incidence, with a small rise for NACA 2412 from 12° to 16°. At 0 degrees, the coefficients are 0.0433, 0.0275, and 0.0300 for NACA 2412, NACA 2415, and NACA 2418. At 16 degrees, they become 0.0155, 0.0120, and -0.0062. NACA 2418 crosses zero between 8 degrees and 12 degrees, while the other two profiles remain positive in the sampled range. The saved convention is positive rotation about +z, with the moment centre at one-quarter chord. The values describe the present cases and do not establish a validated stability characteristic [1].

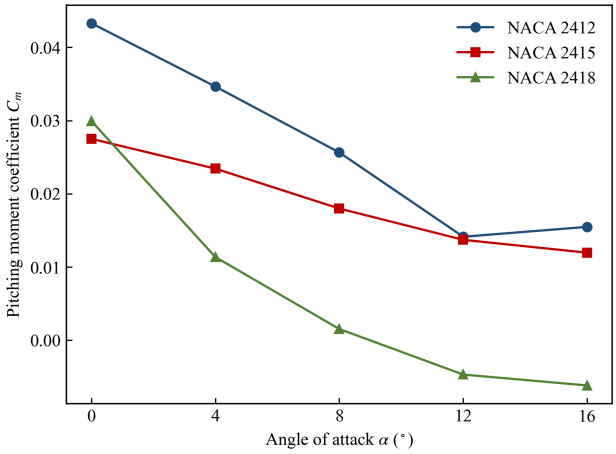


Figure 7. Variation of pitching moment coefficient about the quarter-chord point with nominal angle of attack for the NACA 2412, 2415, and 2418 airfoils at Re = 2.09 × 10^6

3.4. Contextual comparison with reported wind tunnel data

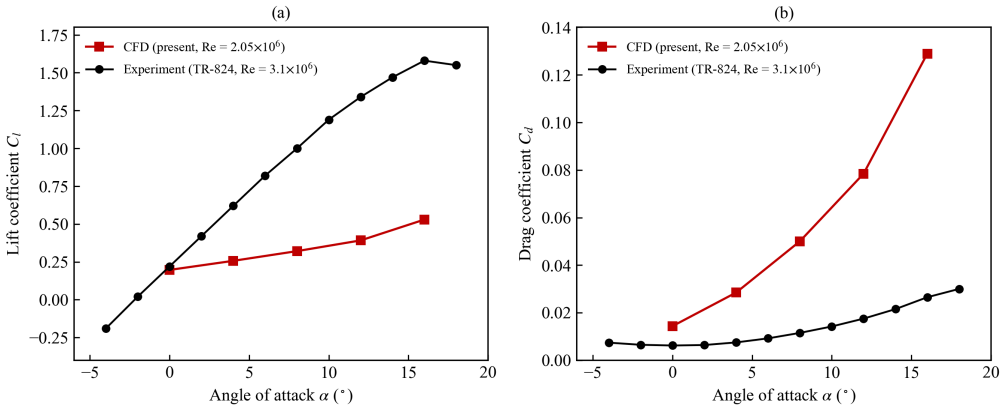


Figure 8. Previously assembled NACA 2412 comparison curves attributed to TR-824 [3], Re ≈ 3.1 × 106, and the present calculations at Re ≈ 2.09 × 10^6. Experimental digitization and polar conversion remain unverified

NACA TR-824 provides the experimental context [3], and UIUC provides geometry coordinates only [8]. Figures 8 and 9 retain the previously assembled comparison plots attributed to these NACA data. The digitized points and the conversion from C_d–C_l polars to C_d–α curves have not

DOI: 10.54254/2755-2721/2026.38955

been independently established, so the plots are contextual and are not used as quantitative validation. The preprint [12] supplies computational-dataset context, not wind-tunnel measurements.

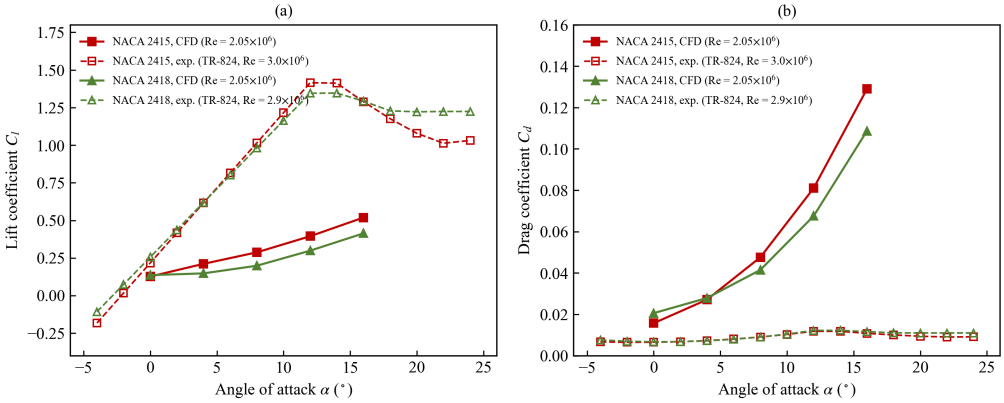


Figure 9. Previously assembled NACA 2415 and 2418 comparison curves attributed to TR-824 [3], at Re ≈ 3.0 × 10^6 and 2.9 × 10^6, respectively. Original plotted points are retained for context; corrected final-iteration values are in Table A1

Table 4 retains the previously reported reference values for transparency. Against those entries, the minimum-drag differences are approximately +131%, +143%, and +203% for NACA 2412, 2415, and 2418. These percentages are arithmetic comparisons of the displayed numbers, not validated simulation errors. The numerical lift maxima are only the largest values among five sampled cases; the numerical stall angles are undetermined.

The nominal numerical Reynolds number is 2.09 million, whereas the attributed NACA curves are near 2.9–3.1 million. Differences in transition and surface condition can also matter [3, 9]. However, the experimental mismatch cannot be assigned to these physical differences alone: sparse surface grids, incompatible inclined far-field constraints, and incomplete iterative convergence remain unresolved in the present calculations.

A reproducible experimental comparison requires documented source pages, curve selection, digitization points, and any conversion between drag polars and angle-of-attack curves. Until that record is established and the numerical sensitivities are assessed, the comparison does not demonstrate quantitative accuracy or reliable relative performance. The reference maxima and minima in Table 4 are retained as reported values pending that check.

Table 4. Sampled numerical extrema and previously reported experimental reference values pending digitization verification. Differences = 100 × (Numerical − Reference)/Reference; they are not validated errors

Parameter	Numerical sample	Reported reference	Difference (%)
	NACA 2412		
$C_{l,\max}$	0.530	1.58	-66.5
α_{stall} (°)	Undetermined	16	—
$C_{d,\min}$	0.0143	0.0062	+130.6
$K_{\max}$	13.7	89.1	-84.6

DOI: 10.54254/2755-2721/2026.38955

Table 4. (continued)

	NACA 2415		
$C_{l,\max}$	0.519	1.41	-63.3
α_{stall} (°)	Undetermined	12	—
$C_{d,\min}$	0.0158	0.0065	+143.1
$K_{\max}$	8.0	119.7	-93.3
	NACA 2418		
$C_{l,\max}$	0.414	1.35	-69.3
α_{stall} (°)	Undetermined	14	—
$C_{d,\min}$	0.0206	0.0068	+202.9
$K_{\max}$	6.6	111.1	-94.1

Figure 10 uses signed tangential wall shear at the saved wall faces. Positive C_f denotes shear toward increasing x along the local surface tangent. At the highest nominal incidence, negative upper-surface samples occur in all three cases, indicating locally reversed wall shear in the saved solutions. Sparse sampling and iterative oscillations prevent a precise separation or reattachment location from being established. The curves therefore describe the archived wall field rather than a converged separation pattern.

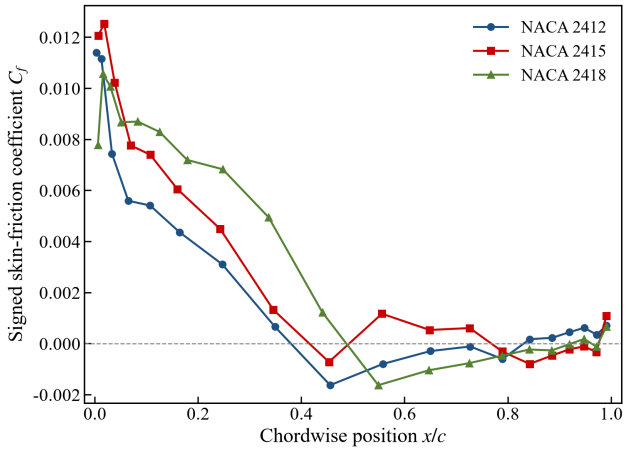


Figure 10. Signed upper-surface C_f from the saved wall-face shear at nominal α = 16° and Re ≈ 2.09 × 10^6. Negative values denote reversed tangential shear; lines connect discrete samples

3.5. Engineering implications and limitations

Within the saved cases, NACA 2412 has the largest K and NACA 2418 the lowest drag at the highest nominal incidence. NACA 2415 is close to NACA 2412 in lift at 12° and 16°. These observations are not yet sufficient to recommend a structural or aerodynamic compromise. The present calculations contain no structural analysis, and numerical errors may change the apparent aerodynamic ranking.

The main limitations are the 38–41 wall faces, unquantified grid sensitivity, persistent equation residuals and coefficient oscillations, and the horizontal symmetry boundaries used with inclined

DOI: 10.54254/2755-2721/2026.38955

inlet flow. The NACA 2418 highest-incidence inlet also differs slightly from the other cases. These effects can influence both absolute values and differences among profiles. Two-dimensional steady RANS further excludes finite-wing effects and resolved unsteady separation. No validated design ranking or stall limit follows from the current dataset.

The next numerical checks should use outer boundaries compatible with the intended freestream, consistent velocity components, and refined surface, wake, and wall-layer meshes. Grid and domain sensitivity should be assessed before repeating all cases. Residual, force, moment, and mass-balance histories should be examined together. If high-incidence flow requires an unsteady treatment, time-step and averaging-window sensitivity must be evaluated. A traceable, matched-condition comparison with the NACA measurements should then assess accuracy.

4. Conclusion

Saved steady SST k–ω calculations for NACA 2412, NACA 2415, and NACA 2418 have been compared at nominal Re ≈ 2.09 × 10^6 over nominal 0°–16°. The final-iteration integrated coefficients are traceable to the case/data files and monitor histories. Density, coupling, gradient settings, mesh statistics, and the NACA 2415 coefficient at 4° have been corrected to match those records.

In the recorded dataset, minimum C_d increases from about 0.014 to 0.016 and 0.021 as thickness rises. At the highest nominal incidence, C_l is approximately 0.53, 0.52, and 0.41. NACA 2412 has the highest K, while NACA 2418 has the lowest drag at that endpoint. The pressure and signed skin-friction samples describe the corresponding wall fields. These patterns remain provisional because their sensitivity to the mesh, boundary conditions, and iterative convergence has not been resolved.

NACA TR-824 provides experimental context [3], and UIUC provides geometry reference coordinates [8]. The current evidence does not establish quantitative experimental agreement or a dependable thickness ranking. Refinement and boundary-condition checks, improved convergence assessment, and reproducible experimental data extraction are required before these calculations can support an airfoil design recommendation.

References

[1] Anderson, J. D. (2017). *Fundamentals of aerodynamics* (6th ed.). McGraw-Hill Education.
[2] Abbott, I. H., & von Doenhoff, A. E. (1959). *Theory of wing sections: Including a summary of airfoil data*. Dover Publications.
[3] Abbott, I. H., von Doenhoff, A. E., & Stivers, L. S., Jr. (1945). *Summary of airfoil data* (NACA Report No. 824). National Advisory Committee for Aeronautics. https://ntrs.nasa.gov/citations/19930090976
[4] Gao, C., Jia, Y.-Y., & Liu, Q.-K. (2020). Effect of relative thickness on aerodynamic performance of airfoil. *Engineering Mechanics, 37*(S), 380–386. https://doi.org/10.6052/j.issn.1000-4750.2019.04.S062
[5] Keskin, S., Ayvazoğlu, M., Sincar, M., Sezer, E. A., Açıkel, H. H., & Genç, M. S. (2023). Effect of airfoil thickness on flow over the cambered airfoils. In *2023 10th International Conference on Recent Advances in Air and Space Technologies (RAST)* (pp. 1–7). IEEE. https://doi.org/10.1109/RAST57548.2023.10197923
[6] Ma, D., Zhao, Y., Qiao, Y., & Li, G. (2015). Effects of relative thickness on aerodynamic characteristics of airfoil at a low Reynolds number. *Chinese Journal of Aeronautics, 28*(4), 1003–1015. https://doi.org/10.1016/j.cja.2015.05.012
[7] Khan, S. H., Danish, M., Ayaz, M., Husain, A., Saeed, S., Abdulla, S., Shaheen, S., Saeed, A., & Thaher, A. (2025). Aerodynamic analysis and ANN-based optimization of NACA airfoils for enhanced UAV performance. *Scientific Reports, 15*, 11998. https://doi.org/10.1038/s41598-025-95848-4
[8] Selig, M. S. (n.d.). UIUC airfoil coordinates database. *University of Illinois Urbana-Champaign*. Retrieved October 2, 2026, from https://m-selig.ae.illinois.edu/ads/coord_database.html

DOI: 10.54254/2755-2721/2026.38955

[9] Menter, F. R. (1994). Two-equation eddy-viscosity turbulence models for engineering applications. *AIAA Journal, 32*(8), 1598–1605. https://doi.org/10.2514/3.12149
[10] Ives, R., Keir, A. S., Bassey, E., & Hamad, F. A. (2018). Investigation of the flow around an aircraft wing of section NACA 2412 utilising ANSYS Fluent. *INCAS Bulletin, 10*(1), 95–104. https://doi.org/10.13111/2066-8201.2018.10.1.10
[11] Alsahlani, A. A., Al-SAAD, M., & Al-Mosallam, M. (2023). A study of impacts of airfoil geometry on the aerodynamic performance at low Reynolds number. *International Journal of Mechanical Engineering and Robotics Research, 12*(2), 99–106. https://doi.org/10.18178/ijmerr.12.2.99-106
[12] Agarwal, K., Vijaykrishnan, V., Mohanty, D., & Murugaiah, M. (2024). A comprehensive dataset of the aerodynamic and geometric coefficients of airfoils in the public domain [Preprint]. *Preprints*. https://doi.org/10.20944/preprints202403.0896.v1

DOI: 10.54254/2755-2721/2026.38955

Appendix

Table A1 lists final-iteration coefficients from the saved case/data and monitor histories. The iteration is 4000 except for NACA 2415 at nominal 8° (4239). K is calculated from unrounded C_l and C_d. Nominal angles are used; the NACA 2418 case labelled 16° has a saved inlet angle of 15.857°. These are archived values, not independently converged performance data.

Table A1. Saved final-iteration aerodynamic coefficients at nominal angles of attack

α (°)	C_l	C_d	$K = C_l/C_d$	C_m
NACA 2412				
0	0.197	0.0143	13.74	0.0433
4	0.257	0.0285	9.03	0.0347
8	0.321	0.0500	6.42	0.0257
12	0.392	0.0785	5.00	0.0141
16	0.530	0.1289	4.11	0.0155
NACA 2415				
0	0.127	0.0158	8.04	0.0275
4	0.209	0.0271	7.69	0.0234
8	0.288	0.0476	6.04	0.0180
12	0.395	0.0810	4.87	0.0137
16	0.519	0.1290	4.02	0.0120
NACA 2418				
0	0.136	0.0206	6.59	0.0300
4	0.148	0.0279	5.29	0.0114
8	0.199	0.0415	4.79	0.0015
12	0.299	0.0676	4.42	-0.0047
16	0.414	0.1087	3.81	-0.0062